3D PRINTING AND ADDITIVE MANUFACTURING
Volume 3, Number 4, 2016

DOI: 10.1089/3dp.2016.0037

ORIGINAL ARTICLE

Local Viscosity Control Printing for High-Throughput Additive Manufacturing of Polymers

Joshua E. Siegel, Dylan C. Erb, Isaac M. Ehrenberg, Pranay Jain, and Sanjay E. Sarma

Abstract

Fused deposition modeling's (FDM) throughput is limited by process physics as well as practical considerations favoring single-head polymer extrusion. To expedite the thermoplastic additive manufacturing process, we propose a parallelized material deposition process called local viscosity control (LVC) additive manufacturing. LVC prints an entire layer in one step by selectively modulating the viscosity of polymer feedstock in contact with a heated wire mesh. Layers of molten polymer are contact printed, with the relative motion between the wire mechanism and a build plate allowing wetting and surface tension to transfer selectively heated, lower viscosity regions of polymer to a fixed substrate. Experiments demonstrate the viability of this process using a single cell depositing layered polycarbonate pixels. Theoretical analysis shows this process may offer similar capabilities in resolution to conventional FDM with a significantly higher production rate for commonly available input power.

Keywords: additive manufacturing, rapid prototyping, fused deposition modeling, high-throughput manufacturing processes

Introduction

Over the last few decades, additive manufacturing processes such as fused deposition modeling (FDM) have matured, with decreasing costs and substantial improvements in maximum build volume, feature resolution, and available material properties. Despite this progress, there remain challenges to thermoplastic additive manufacturing's widespread use for the fabrication of everyday objects. In particular, poor throughput poses a significant obstacle to FDM viability in high-volume, high infill prototyping and mass manufacturing.

Commercially available FDM systems have limited construction speeds due to the thermoplastic build material's intrinsic properties and the physics governing FDM.[1] Moderating factors include the convective and conductive heat transfer properties of the polymer and the mass of the printer head, and this limits the speeds at which the printer head can operate and dominates the axial driver sizing required to achieve acceleration and speed targets. To allow the creation of high-resolution parts, FDM extruder nozzles feature reduced diameters, enhancing precision at the cost of further constraining production rate. These factors constrain FDM applicability to slow-turn prototyping and low-volume production.

A higher rate extrusion system, even one sacrificing quality, would enable novel applications of additive manufacturing for higher volume production and could create a sense of instant tangibility conducive to consumer use. Although multiextruder systems today increase production rates, improvements are marginal, control software is complex, and the fundamental process remains constrained by physical and mechanical rate limits. Simplified and massive parallelization is needed to revolutionize throughput.

In traditional FDM with unlimited material supply and demand, the extruder's flow rate and transit speed govern production rate. Each additional extruder adds to the throughput volume in equal measure, allowing simultaneous material deposition in several locations. Allowing each extruder to operate in a smaller region lessens axis acceleration requirements and reduces transit time. Extending the concept of parallel heads to the limit of one head per ''pixel,'' in-plane motion may be eliminated entirely. Reducing the extruder's need for motion to a single vertical axis simplifies

Massachusetts Institute of Technology, Cambridge, Massachusetts.

a printer's mechanical design, making it less expensive and more reliable.

This article explores throughput improvements in FDM and introduces the concept of local viscosity control (LVC) printing, which extends FDM to its parallelized limit. LVC is an additive manufacturing process for printing an entire layer of a three-dimensional (3D) part in a single step. The concept's introduction is followed by a discussion of its mechanics, demonstration of a benchtop experiment, and future directions.

Related Work

From its introduction until 1998, FDM had increased in speed by up to 500%,[2] although consumer systems sold today still rarely exceed 250 $\frac{mm}{s}$ in axial travel speed. Extruder mass and heat transfer increase the complexity and limit the benefit of continued speed improvements in extruder design, while this axial speed restriction limits deposition rate and is a known constraint within the industrial and research communities.

Partially addressing this concern, new additive manufacturing systems feature multiple extruders for multimaterial construction, or parallel deposition of identical material. Designs include jointly moving heads or independent motion control, increasing throughput along with hardware cost and software complexity.[3]

Another approach to throughput enhancement uses variable nozzle diameters, with a single, variable aperture extruder head capable of laying down filaments of various sizes. These extruders quickly traverse resolution-insensitive portions of the build while shrinking and slowing to provide additional detail in complex regions.[4] This method allows part surface quality to be maintained while increasing overall throughput. However, uniformly high-resolution parts will still face the same rate limit as in the fixed aperture extruder case.

Although we choose to examine the FDM due to its wide use today and the availability of varied input materials, other additive techniques, such as stereolithography (SLA), suffer from similar rate-limiting serialization. In SLA, a small volume of photopolymer is targeted with light to induce localized crosslinking. As in the multiextruder FDM case, advanced SLA systems include multiple laser sources, improving the production rate by crosslinking numerous regions simultaneously.[5]

Parallelism and rapid prototyping coincide in digital light projection (DLP) 3D printing, a process similar to SLA. In a DLP system, an array of mirrors project light onto a vat of photopolymer, exposing all the necessary regions simultaneously and constructing the part one layer at a time. This works with specialized photocurable polymers, although no similar system has yet been used with the more desirable thermoplastics used in FDM.[6]

Recently, a number of techniques for wide area material deposition have emerged. ''Binder jetting'' and similar proprietary technologies such as Stratasys PolyJet and HP's Multi Jet Fusion offer higher throughput than FDM and SLA with similar resolution limits and material properties. We consider Multi Jet Fusion in examining this type of drop- and voxel-based, high-throughput technology.

Multi Jet Fusion is a multistep additive process relying on biaxial motion and material deposition to form 3D parts. In Multi Jet Fusion, raw material is first deposited along one axis of motion to form a bed. Chemical curing and finishing agents are then deposited from a thermal inkjet array traversing the perpendicular axis, varying the dispersion of several different types of chemicals based on the needed geometry and material properties. Finally, energy is added to the chemical-infused materials, with the material curing in regions where fusing chemicals have been added. This results in the formation of a solid part[7] with material properties varied on a voxel-by-voxel basis. Unfused material remains to serve as support material, but is eventually cleaned and removed.

Relative to FDM and SLA, which rely on a rastering process, this approach is faster because the deposition and solidification processes occur as the result of wide-area lateral sweeping motions. These sweeps apply material, modifiers, and energy rapidly and without dependence on part complexity or area, allowing each layer to be produced nearly in parallel and more rapidly than a ''part tracing'' process such as FDM. Multi Jet Fusion's production approach reduces the distance traveled by each axis, while alternating the direction of travel between layers furthers reduced production time. Despite obvious advantages in production rate, this process still requires triaxial motion, maintaining machine complexity and cost at a high level.

This technique also scales well as additional thermal arrays may be added to expand the printable region, while the build time does not increase significantly—irrespective of array size, a single sweep across the build platform is all that is required for each step. In extreme cases, the mass of additional thermal arrays or other deposition elements may limit maximum acceleration of the carriage, slightly diminishing throughput.

HP marketing materials claim a resolution limit of 2400 DPI, or 11 μm, which offers finer granularity than most extrusion processes. Today, only nylon is printable, although early technical documents suggest the easy interchange of materials and eventual material variability within a single printed layer.

Following this approach of wide area, sweepable print heads is the concept of massively parallel nozzles for material deposition. One embodiment uses microvascular arrays of nozzles to deposit build material.[8] This system relies on linear traversal of a wide nozzle to deposit layers of ink-like fluids. This approach can sweep at 1 m/s and supports nozzle widths of 200 μm. This setup still requires biaxial motion to complete its sweeping deposition and layer change motions, requiring complex machine design and additional transit time relative to stationary, full-area extruders.

These approaches build on FDM and SLA ''point'' extrusion to create ''linear'' extrusion techniques, whereas a complete ''plate'' extruder would eliminate additional axes of motion and transit time, simplifying machine design, reducing cost and complexity, and reducing build time.

LVC Printing

In an effort to achieve maximum throughput using conventional thermoplastics, we designed, prototyped, and tested a new form of 3D printing capable of ''extruding'' an entire layer of material in parallel. Selective material deposition allows an arbitrary 2D array of polymer pixels to be

deposited simultaneously, requiring less time per layer and eliminating the need for horizontal motion control hardware.

To selectively deposit material, LVC takes advantage of the dependence of a polymer's viscosity and shear modulus on temperature, which is the same material property that is integral to FDM and other extrusion-based additive manufacturing. With rising temperature, amorphous polymers such as acrylonitrile butadiene styrene (ABS) undergo glass transition and eventually melt. Past glass transition, the shear modulus decreases sharply,[9] reducing the force required to push or draw the material through a nozzle. LVC precisely controls the viscosity by modulating temperature to ultimately allow low-force, massively parallel thermoplastic deposition.

LVC uses a wire mesh as 2D array of ''nozzles,'' where each nozzle is a fixed aperture wire cell, as shown in Figure 1. The polymer's temperature, and therefore viscosity, is controlled by selectively heating the wire(s) in proximity with the location where deposition is desired. When all four edges of a cell are heated, the ''pixel'' receives enough heat to transition to a viscous melt and begins to droop under its own weight or an externally applied pressure. This heating process is shown in Figure 2.

To facilitate a rapid transition between the viscous melt and hard solid states, the plastic feedstock is maintained in a ductile and deformable state at a temperature just below the melting point.[10] This characteristic allows the feedstock to be maintained without substantial fluid flow. When the temperature is increased, the sharply reduced viscosity in the fluid allows the polymer to droop through the mesh due to the force of gravity or applied pressure, forming a convex meniscus. This meniscus forms below the mesh and provides a protruding surface capable of wetting and adhering to a substrate for contact printing, as shown in Figure 3.

After contact is made, the heating source is switched off, returning the feedstock to a lower resting temperature. This causes the remaining polymer to cease flowing, preventing further meniscus formation until the feedstock can be replenished, for example, by liquid recoating or solid material replacement. Gravity, applied pressure, and surface tension force the polymer to separate from the wire mesh and adhere to the substrate as the mesh and build platform move apart.

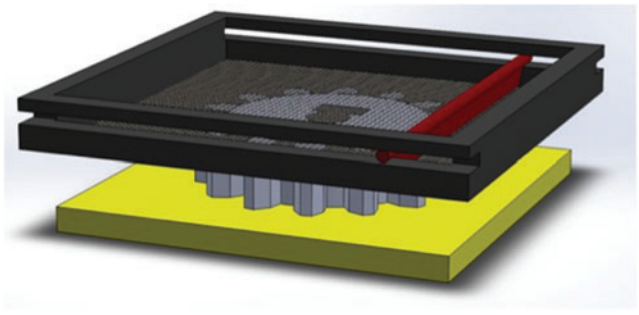

FIG. 1. A representative series of mesh ''nozzles'' capable of depositing a three-dimensional part onto a substrate. This plate-style configuration eliminates the need for lateral motion, instead requiring only a single moving axis to vary distance between the mesh apertures and the build surface. A ''squeegee'' type recoating mechanism for feedstock polymer is shown in *red*. Color images available online at www.liebertpub.com/3dp

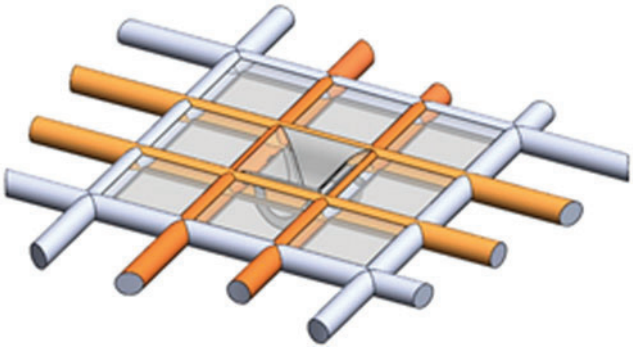

FIG. 2. The mesh is selectively heated to provide input energy capable of transitioning the polymer to a flowable state. Here, four wires are engaged to transition the single central cell for deposition. Neighboring cells are kept slightly below the flowable transition point for the given polymer. Color images available online at www.liebertpub.com/3dp

Electrical heating provides a simple means of modulating polymer viscosity. In principle, the details of the mesh such as its size, wire diameter, wire coating, and opening widths can be chosen so as to minimize any externally applied pressure required to make the liquid polymer droop through the aperture, while at the same time minimizing sensitivity and unintentional heating of neighboring cells.

A set of example LVC nozzle meshes operating through electrical heating is shown Figure 4. These have a simple design consisting of a single-nozzle nichrome grid to be heated uniformly. Figure 5 shows the extrusion process in a canonical case. The extruder begins by engaging the wires appearing in orange and heating those edges. The cells bounded entirely by orange are brought above the melting point, while the other cells receiving fewer than four heated edges are kept below this temperature. The process continues, and the cells sweep across the intended pattern rapidly to allow for bulk material heating before contact printing. The use of per-wire heat control allows n^2 cells to be controlled with $2n$ total actuators, greatly simplifying the control electronics.

One side effect of per-wire heat control is that engaging multiple nearby wires may result in heating of a cell not intended for printing (e.g., two cells activated with a central cell deactivated). In such a case, a serial addressing schema is necessary to reduce or eliminate unanticipated prints. Provided the time constant for cooling of the wires is much less than that of the polymer, a single contact step may be used to separate every fluid drop in parallel despite rapid serial wire heating.

The LVC XY stationary extruder design eliminates the need for a heavy motor on the extruder as well as the need for lateral axial motion, simplifying the mechanical complexity of the printer. These simplifications, along with the massively parallel arraying of heaters, allow us to bypass the mechanical and thermal rate limits of conventional FDM, SLA, binder jetting, and micronozzle arrays. The lack of motion further simplifies scaling the print area, as acceleration, vibration, and motor weight and power are not concerns. In the subsequent sections, we derive theoretical limits on the minimum practical pixel size and experiment with a single cell to validate the concept of LVC as an improvement on existing additive technologies.

FIG. 3. The heated polymer forms a bulging convex meniscus protruding through the mesh. Here, a *dotted line* represents the build surface's substrate that will come in contact with the meniscii during printing, allowing the polymer to wet and adhere to the base material. Color images available online at www.liebertpub.com/3dp

Limits on Resolution

To find the fundamental resolution limit of the LVC printing process, we examine the contact mechanics of a single cell during printing. As illustrated in Figure 6, we assume a catenoid shape to approximate the molten polymer bridge that extends between the wire mesh and the print substrate during printing.

To derive the limits of resolution, we make a few simplifying assumptions. One key assumption is that the polymer enclosed in a cell is uniformly heated to a temperature above the melting point. This is justified at finer resolutions as the distance for thermal conduction decreases, resulting in near-constant temperature across the entirety of the polymer. We recognize that at coarse resolutions, the heat will be concentrated closer to the edges and this model may fail to be accurate. In this case, the heating should still provide sufficient flowability to allow for drooping and adhesion, although the input energy requirements and heating time will change, as will the geometry of the deposited material.

Returning to the fully melted model, the main forces of concern are the surface tension (γ) at the interface between the wire mesh and the liquid bridge (F_1), the surface tension at the perimeter of the contact patch (F_2), and the weight (W) of the bridge itself.[11] An optional external load (P) applied at the top of the catenoid balances the forces with a pressure required to maintain static equilibrium. This is a pressure that may be applied to help the molten polymer separate from the mesh and deposit on the print substrate. This pressure may be applied in a number of ways; for example, a jet of air could be used to apply pressure to the top surface of the material on the mesh and thus the catenoid, or else P may be a hydrostatic pressure depending on how the initial material stock is deposited. The relationship between all the forces in the z direction is as follows:

$$F_1 = F_2 + W + Pd^2.$$

The revolved profile of the catenoid follows the hyperbolic cosine function:

$$r(z) = a\cosh\left(\frac{z}{a}\right).$$

When considering the boundary conditions on the single polymer cell, it was assumed that the wire mesh acts as a fixed width support at the upper end of the catenoid while maintaining a radius of $\frac{d}{2}$ at this location. While in our implementation, the mesh is square rather than round, the approximation

$$r(z_d) = a\cosh\left(\frac{z_d}{a}\right) \approx \frac{d}{2}$$

suffices to predict the average angle of surface tension around the perimeter of the wire.

With this boundary condition, the z position at which $r(z) = \frac{d}{2}$ is as follows:

$$z_d = a\cosh^{-1}\left(\frac{d}{2a}\right),$$

and the derivative of the shape function with respect to z is

$$\frac{dr}{dz} = \sinh\left(\frac{z}{a}\right).$$

The average contact angle of the molten polymer bridge with the wire is then

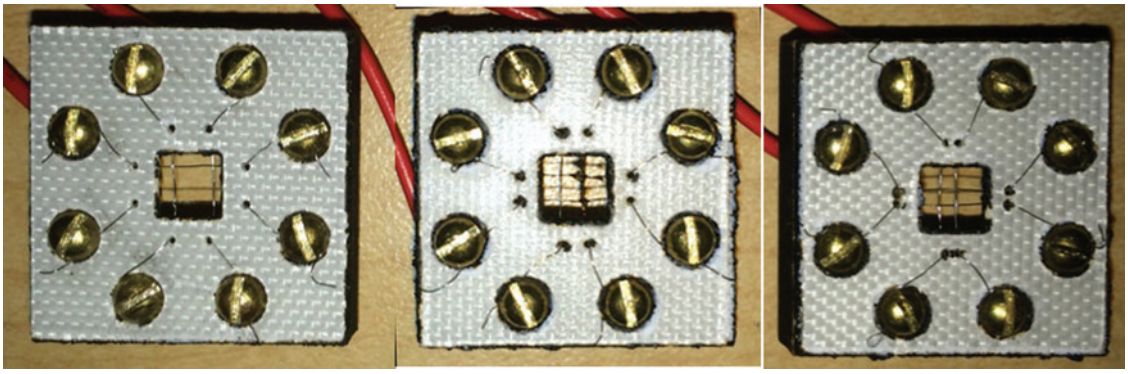

FIG. 4. To demonstrate meniscus-generating heating, example meshes were constructed from garolite, MDF, and fiberglass-coated nichrome wire. From *left* to *right*, these cells show 1, 2, and 3 mm central apertures. MDF, medium density fiberboard. Color images available online at www.liebertpub.com/3dp

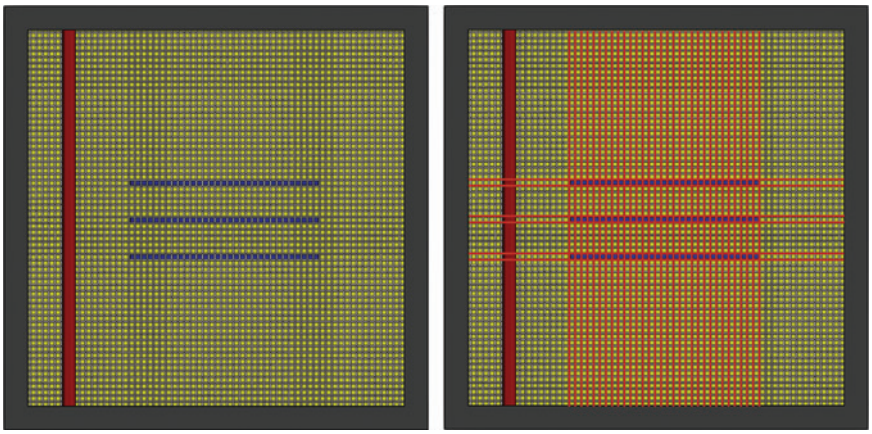

FIG. 5. In this figure, we render the desired material deposition in *blue* on the *left*. On the *right*, *orange* lines highlight the wires that must be activated to appropriately heat the polymer for deposition. In cases, this heating must be staggered to avoid accidental deposition of cells that might otherwise be heated at all four edges. Color images available online at www.liebertpub.com/3dp

$$\theta_d = \cot^{-1}\left(\sinh\left(\cosh^{-1}\left(\frac{d}{2a}\right)\right)\right).$$

At the interface between the liquid bridge and the printed material substrate, the liquid will maintain a constant contact angle of θ_i.[12] The cotangent of θ_i must be the slope of the shape function at the point of contact, making the z position of contact the following:

$$z_i = a\sinh^{-1}(\cot\theta_i)$$

Therefore, $r(z_i)$ is as follows:

$$r(z_i) = a\cosh\left(\sinh^{-1}(\cot\theta_i)\right).$$

With the shape function and the boundary conditions known, the volume of the liquid bridge can be calculated by taking the integral as follows:

$$V = \int_{z_d}^{z_i} \pi\left(a\cosh\left(\frac{z}{a}\right)\right)^2 dz$$

which simplifies to the following:

$$V = \frac{\pi a^3}{4}\left(\sinh\left(\frac{2z}{a}\right) + 2z\right)\Big]_{z_d}^{z_i}.$$

If we assume that the plastic starts above the mesh with a thickness of $\frac{d}{10}$, the volume of the liquid bridge can be set equal to $\frac{d^3}{10}$:

$$\frac{d^3}{10} = \frac{\pi a^3}{4}\left(\sinh\left(\frac{2z}{a}\right) + 2z\right)\Big]_{z_d}^{z_{\theta_i}}$$

For any given values of d and θ_i, a value of a can be selected, which satisfies the above volumetric equation. This fully defines the catenoid and allows the applied pressure to be derived:

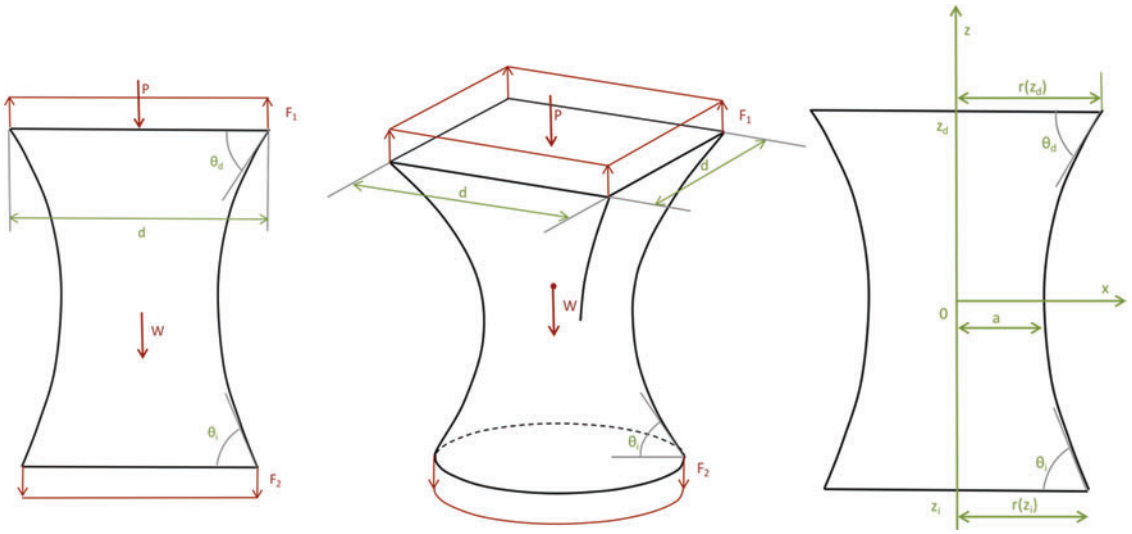

FIG. 6. The molten polymer bridge between a wire mesh cell and the substrate is assumed to take the shape of a catenoid. *Red arrows* indicate the forces acting on the bridge and *green arrows* are projection lines that indicate dimensions. Color images available online at www.liebertpub.com/3dp

$$P = \frac{4d\gamma \sin\theta_d - \rho g V - 2\pi\ r(z_i)\gamma \sin\theta_i}{d^2}.$$

When this pressure is plotted against the range of mesh sizes and contact angles as in Figure 7, an asymptotic increase in pressure emerges as the wire spacing approaches zero. When the aperture dips below 0.1 mm, significant additional positive pressure P must be applied to ensure the molten polymer transfers from the wire mesh to the print substrate. From a practical standpoint, large increases in pressure will quickly complicate the design of the apparatus, increase cost, and act as a cap on the achievable print resolution for the majority of use cases.

Limits on Throughput

While the LVC theoretical resolution limit of 0.1 mm is similar to that which has been successfully demonstrated by FDM equipment,[13] LVC does have an advantage over FDM when it comes to material deposition rates. The extrusion rate for conventional, single-nozzle FDM manufacturing is dependent on many factors, including nozzle geometry, system heat transfer characteristics, and the available extrusion force. Practical constraints, such as system size, complexity, and ultimately cost, limit the volumetric flow rate on commercial FDM systems to volumes on the order of $0.32\,\frac{\text{m}^3}{\text{yr}}$ (this rate is estimated based on an FDM printer with input material diameter of 1.75 mm, a feed rate of $250\,\frac{\text{mm}}{\text{min}}$, and an extrudate diameter of 0.25 mm). LVC is a similarly complex material deposition system and while its volumetric throughput rates are also heavily dependent on material properties and design parameters, our analysis shows that by making some reasonable physical assumptions about LVC, the process's inherent parallelism can be exploited to reach significantly higher material deposition rates.

We aim to demonstrate LVC improvement over FDM by examining the time taken for each step in the LVC deposition process. To model the maximum deposition rate of LVC, the process is broken down into constituent steps of heating, lowering, dwelling, raising the platform, and recoating. All of these processes except heating and recoating are invariant in time with respect to printed area, and changes in coating time are likely to be negligible relative to the rest of the printing process.

Based on an experimental setup we built (discussed in a later section), we were able to determine typical times for the invariant processes. Using tests resulting in successful deposition as the basis for our model assumptions, we determined that a typical transit time for the vertical axis is on the order of 2 s (1 s up, 1 s down). The low transit speed is to ensure that the deposition and separation of the material is predictable and unperturbed by machine vibration. Dwell time of one half second worked well in testing to allow the material to deposit and cool appropriately before separation.

Coating times may vary, but we assume that 1 s is a reasonable estimate. This is based on the time it took for us to manually deposit fresh material on the print mesh between deposition events. A liquid recoating mechanism may be faster still.

The only time that is not accounted for in these estimates is the heating time, which may vary based on power inputs and melt temperatures. We will calculate this next.

From these assumptions, we see that there is a fixed time of 3.5 s per layer (transit + dwell + recoating), plus the time to heat the polymer. This heating time (the time to bring the polymer across the glass transition temperature) is limited by input power, which we set to $P_{in} = 1500$ W, similar to the maximum power drawn by many home appliances. By calculating this time, we will be able to get an accurate estimate of the LVC maximum theoretical deposition rate.

For a first-order calculation, heat exchange between the polymer and mesh may be modeled as 1D conduction through a thin film or slab of polymer. In an example case, plate dimensions are taken to be $L = W = 100$ mm and thickness taken to be $t = 0.1$ mm. Edge effects are ignored, and 99% of mass is assumed to transfer on contact, with the remainder lost due to

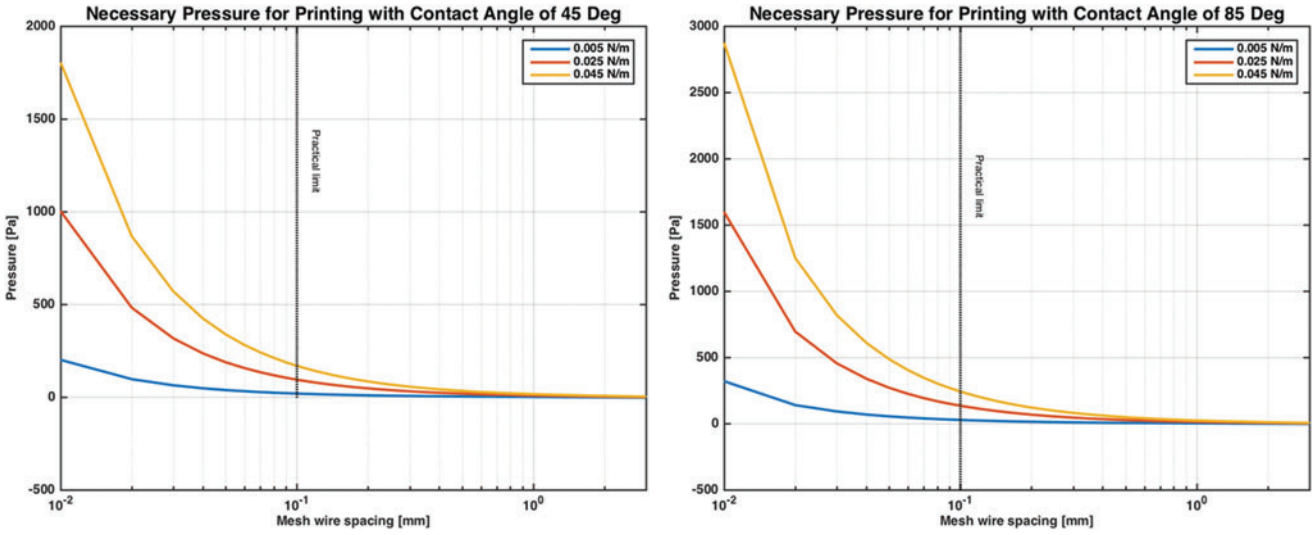

FIG. 7. These plots show that the applied pressure necessary for printing is a function of the mesh size, the contact angle between the print substrate and the molten polymer, and the surface tension. Our model predicts that for most contact angles ranging from 45° to 85°, the pressure required for printing will asymptotically rise for apertures smaller than 0.1 mm. Color images available online at www.liebertpub.com/3dp

burned-off impurities, wicking into the wire coating and evaporation (the fiberglass we tested with demonstrated this degree of material loss; other high-temperature wire coatings, such as PTFE, may transfer a higher percentage of the material to the substrate without loss). The material properties are taken from ABS plastic, where the density is $\rho = 1.04 \frac{g}{cc}$. The specific heat used for the calculations was $C_p = 2004\,\mathrm{J/kgK}$. In these calculations, heat of fusion was ignored due to the amorphous structure of ABS and the gradual nature of its phase change.

We assumed the melt temperature of the feedstock at the wire/material interface to be 230°C, a typical extrusion temperature for FDM using ABS. We assumed that the wires heat uniformly and instantaneously. The starting temperature of the polymer deposited on the mesh is $T_i = 95°C$, just below ABS glass transition temperature. Electrical input to thermal transfer efficiency at the polymer interface η_{power} is assumed to be 20%, a rough estimate assuming 80% is lost to conduction and convection between the exposed wire and the surrounding air.

The heat input required is taken from a simple formulation for melt energy:

$$\Delta H = mc_p\Delta T + m\Delta H_f$$

where

$$m = L * W * t * \rho = (100\,\mathrm{mm})^2 * (0.1\,\mathrm{mm}) * \left(1.04\frac{g}{cc}\right) = 1.04\,\mathrm{g}$$

$$\Delta T = 220°C - 95°C = 135°C$$

The heat required is as follows:

$$\Delta H = \left(1.04g * 2004\frac{J}{kgK} * 135°K\right) + (0) = 281.4\,\mathrm{J}.$$

The heat time to melt an entire thin sheet with a deposited build volume of $V_{deposit} = \eta_{transfer} * L * W * t = 990\mathrm{mm}^3$ is

$$t_{melt} = \frac{\Delta H}{P_{in} * \eta_{power}} = \frac{281.4J}{1500\,\mathrm{W} * 0.2} = 0.94\,\mathrm{s}.$$

As the rate is dominated by transit and dwell time, further scaling up of the cell greatly increases production rate, since the additional material heating time remains much less than the transit time.

Using material deposition rate as an input to the cycle time model, the layer time would be

$$t_{cycle} = 3.5s + t_{melt} = 4.44\ s$$

making the theoretical maximum yearly rate.

$$\frac{V_{deposit}}{t_{cycle}} = \frac{990\,\mathrm{mm}^3}{4.44s} = 7.02\frac{\mathrm{m}^3}{\mathrm{yr}}.$$

The plots in Figure 8 show that for this model, there is a critical build area at which LVC matches and then outperforms FDM for a given layer height and power level. When only 15 W is available, FDM and LVC offer similar throughput performance. Once 150 W is used, LVC quickly surpasses FDM, with the crossing point at roughly 2.4 cm per side. For a 1500 W system, LVC performs even better, surpassing FDM at 1.84 cm per side. This finding validates the importance of LVC for large-scale rapid prototyping and highlights the benefits of eliminating the XY actuation of FDM. Note that the asymptotic limit of the extrusion rate is due to a fixed limit for available power, which causes polymer heating time to dominate cycle time in large build areas.

Experimental Setup

We validated the LVC concept empirically using a manually controlled setup. Initially, we conducted cellular-level testing with a range of materials, including common thermoplastics

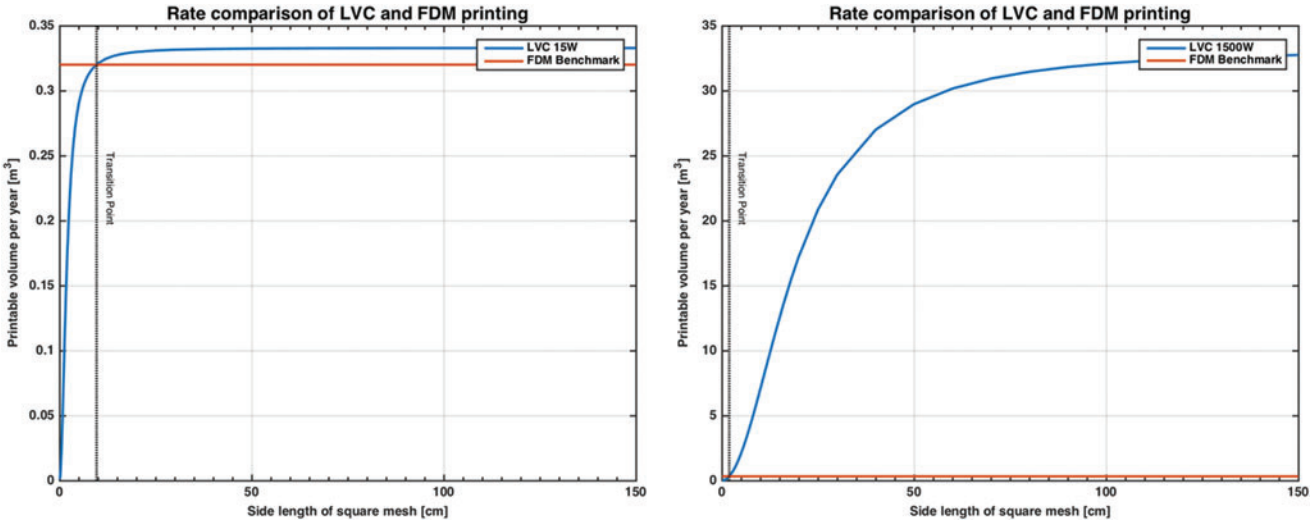

FIG. 8. When comparing the material deposition rates of FDM and LVC, a tradeoff emerges. In situations where power is limited to 15 W, peak FDM and LVC performances are similar. In cases where more power is available, the rate of LVC exceeds that of FDM once the build area crosses a critical threshold. In the case of 1500 W of available power (a typical household outlet), this value is 1.84 cm per side, or 3.39 cm^2. FDM, fused deposition modeling; LVC, local viscosity control. Color images available online at www.liebertpub.com/3dp

such as ABS, nylon, polylactic acid (PLA), and low density polyethylene (LDPE), and tested for successful deposition onto a substrate with and without forced substrate contact during the adhesion stage. In each test, we followed the same process of depositing precut plastic feedstock onto a nichrome wire single-cell mesh, applying current to generate heat at the four edges of the central wire cell, and either allowing the plastic to droop independently or manually moving the cell to make contact between the substrate material and the molten plastic before separating the cell from the substrate. Infrared images outlining the process appear in Figure 9.

After manual testing, we devised a repeatable fixture to study sensitivity of printing to different input parameters. To ensure repeatable contact, we constructed a Z-stage to raise and lower the wire grid predictably during operation. The design included a stepper motor and four belt-driven pulleys mated to two smooth shafts and two threaded rods with driving nuts mounted in compliant flexures to minimize binding.

To perform single-cell experiments, we constructed four varying-size mesh single-cell printers. In each cell, the base plate was laser cut medium density fiberboard (MDF), with a top layer of garolite heat-resistant phenolic fiberglass laminate that was laser cut into a loom. We then wove nichrome wire, both coated and uncoated, through the predefined holes, and wrapped it around the screws. Cell grid sizes ranged from 1 to 3 mm. These sizes were selected for experimentation based on the difficulty of hand manufacturing; weaving the wire proved a challenge. While the larger apertures will not fully melt as in the model, these sample cells are still useful to prove that even localized, edge-only melting is sufficient to allow for successful layer-to-layer adhesion.

These cells were designed to approximate the heat input of a conventional FDM printer, based on an order of magnitude calculation that assumed our output volume per cell and FDM output volume per unit time should be similar. Each cell had a measured resistance of 1 ohm, and during testing the voltage and current fell within the range of 3 V, 3A (9 W) to 4 V, 4A (16 W), similar to the heaters found in consumer FDM printers.

With the test cells fixed to the Z-stage, we developed electronics to control movement and limit current flow through the printing cells. The resulting automated process begins with the Z-platform homing against a limit switch and subsequently returning to a predefined height above the print bed. Depressing the home switch again manually then begins a deposition cycle consisting of heating the nichrome wires of the cell, lowering the platform until the mesh contacts the substrate, then retracting the cell away from the substrate once the polymer has had the chance to adhere. On completion of a single print cycle, the height of the platform is raised to allow printing the next layer on top of the first.

We used software and hardware adjustments to modify several parameters in each deposition experiment, in the hopes that repeated experiments would identify the optimal settings for reliable LVC printing. Parameters varied included dwell time of the contact, duty cycle of nichrome heating, and the contact height. For this prototype, all of the controls were open loop.

Results and Discussion

Experiments gauged the sensitivity of printing to various control parameters based on the success and qualitative output of each print attempt. The use of qualitative metrics was a necessary concession due to limited availability of high-precision measurement equipment capable of capturing size, uniformity, and shape of each deposition.

In early testing, we found polycarbonate to be the most repeatable printed material using our setup, so later experiments were conducted using pieces of 3-mil-thick polycarbonate as inputs. These polycarbonate blanks were placed onto 1, 2 and 3 mm test grid cells (1/8'' diameter pieces for the 1 and 2 mm grids, and 3/16'' for the 3 mm grid), using tweezers after

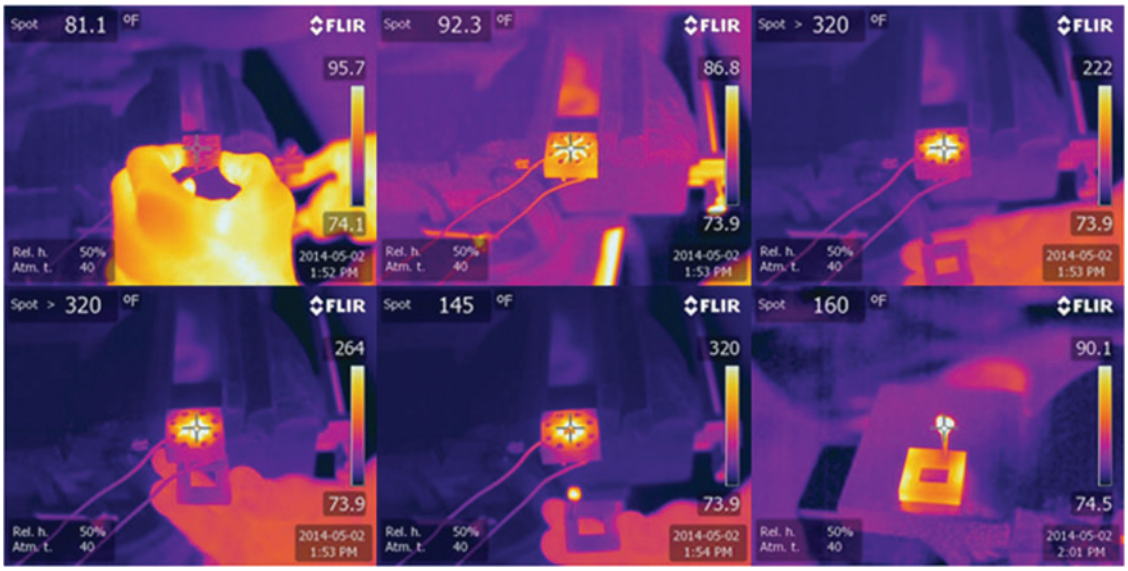

FIG. 9. This figure shows the sequence of contact printing, from heating to drop separation, from *left* to *right* and *top* to *bottom*: the cell before current being applied, the cell activated and the polymer beginning to melt, polymer brought near the heating element, the molten polymer and a heat-resistant substrate (garolite) are placed in contact and left to dwell, separation of the substrate and the heating element, the hardened polymer droplet adhered to the substrate. Color images available online at www.liebertpub.com/3dp

grounding the wire to reduce static interactions. From here, the print process was to heat the blank, make contact with the bed, and retract the mesh with the intent of leaving material adhered to the substrate.

We initially kept records using binary metrics: we chose settings arbitrarily and recorded the experiment as being successful if a visible nugget of material was deposited and adhered to the substrate (adherence was tested using tweezers to manually separate the deposited material; if the material withstood the weight of the tweezers it was considered to be adhered). These tests were completed as a baseline to provide rough starting numbers for input into a later design of experiments, and as the eventual foundation for a process window plot showing acceptable ranges for input parameters to yield a print output. Completing these manually controlled experiments highlighted the complexity of our intended DoE. The simplified input parameters chosen for our testing were nichrome mesh grid size (1, 2, 3 mm), *x*-axis vibration motor activation (off, 6 V), substrate material (garolite, self-adhesion), preheat time (0–15 s), and preheat pulse width modulation (PWM) (0–100%). Other parameters set in software included dwell/contact duration, vibration duration, and heat input during the lowering and separation phases.

Qualitatively, we were able to deposit samples with all of the meshes, but the repeatability increased with aperture width. Stacking multiple prints was also more repeatable with the larger grid size. Although the experiments proved the setup could repeatedly print down to the 1 mm grid size, the resulting output was not predictable. This is likely due to the use of open-loop control and noncoated wire on the 1 mm grid size. Three printed extrusions appear in Figure 10, showing a clean ''pancake'' print, a long ''necked'' print, and a print with a ''tail,'' as described in our test notes. Note that the deposited material shows signs of burning and scorching—these defects are not inherent to the process, but rather are an artifact of our use of open-loop temperature control. The use of infrared imaging or thermocouple-based feedback could limit this in the future.

From these early-stage results, we gained insight into possible future improvements for LVC technology. Vibration during deposition, for example, significantly reduced adhesion by forcing the molten polymer to bounce up and over the mesh rather than down and through. Wire coatings were shown to not only ease assembly of complex multicell meshes but also to improve repeatability over multiple prints, whereas uncoated wires would pick up debris and jam. Testing also highlighted

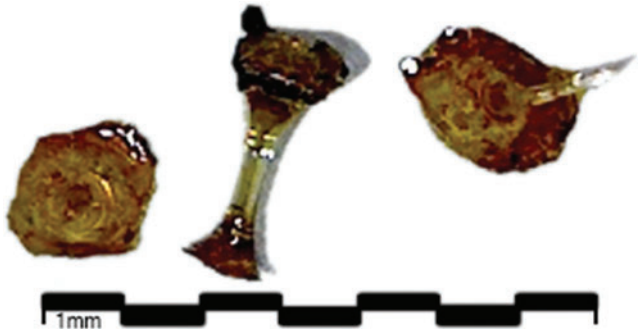

FIG. 10. Three deposited samples demonstrating several types of contact-print outputs with various degrees of uniformity and necking. Color images available online at www.liebertpub.com/3dp

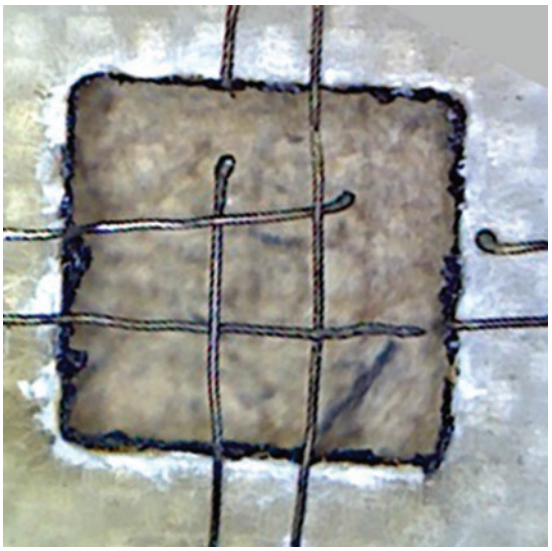

FIG. 11. This nichrome mesh burnt as a result of poor open-loop control, highlighting a potential future design improvement. Color images available online at www.liebertpub.com/3dp

the need for cellular-level closed-loop feedback, to reduce the risk of burning through the mesh (Fig. 11) and to allow more uniform deposition over a range of ambient conditions.

The 3 mm prints highlighted the importance of edge melting and showed that we do not need complete melting of the polymer feedstock to allow for full adhesion. The cell wires at the perimeter act like a hot wire cutter and allow a plastic plug to drop out. In these tests, the drop bound fully to the substrate, allowing an additional two voxels to be deposited above it, as shown in Figure 12.

Since conducting the initial experiment, we have developed an improved test stand. This setup is based off an Arduino MEGA and provides individual control over 12 wires, as well as offering rotary knobs and other input devices to simplify rapid testing. This allows testing of a complete array of cells with individually addressable edges. Temperature

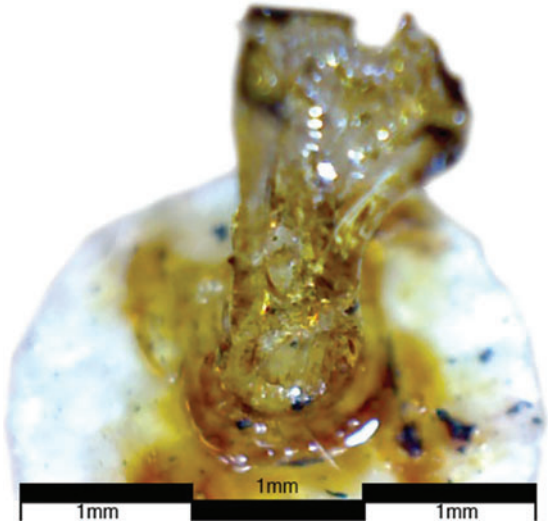

FIG. 12. A three-layer stacked pixel, with a 1/8″ diameter of the white garolite substrate. Color images available online at www.liebertpub.com/3dp

feedback is provided using thermocouples at each wire's edge, with a SEEK Thermal camera used to develop a PC-based visual control system, eliminating the burning issues seen in the manually controlled and open-loop prototypes.

Initial experimentation has shown this test stand to be a valuable tool in rapid classification of materials and wiring configurations. Qualitatively, this device has shown PTFE-coated nichrome to be more resistant and less ''sticky'' than fiberglass-coated, enamel-coated, and uncoated nichrome wire. It has also proven instrumental in examining how shrinkage and expansion impact deposition of different materials.

Future experimentation will apply this test device to examining edge heating's impact on neighboring cells and demonstrating deposition of a single cell while other cells remain in place. We will further extend this setup to explore recoating and other feedstock delivery mechanisms.

Conclusion

FDM wide adoption has been fueled by the commoditization of multiple types of feedstock material, leading to the use of thermopolymer-based extrusion systems in environments ranging from factories to businesses to offices and even homes. It has become the most ubiquitous additive manufacturing system available today, producing high-quality parts and allowing the use of materials with vastly different properties. Despite its successes, this technique faces significant limitations; namely, low production rate, small build volume, and machine noise and complexity. These limitations have kept additive manufacturing from reaching its full potential.

Some FDM implementations have been used successfully in research or industry to produce large parts, including full-scale airplane component mockups or small vehicle bodies in a single build, although building such components requires a significant amount of time and specialized equipment. The same speed and volume constraints apply to other common techniques, such as SLA or binder jetting. There is therefore an opportunity to enable low-cost, high-impact additive manufacturing for the masses by lowering cost and time barriers to entry.

Addressing these issues and bringing the promise of practical additive manufacturing closer to commerce and hobbyists, we presented the concept of LVC 3D printing as an alternative to FDM-based processes. This technique improves on FDM, using the same functional thermoplastic materials but increasing throughput and reducing machine complexity. Through its capacity to deposit thermoplastic polymer pixels in parallel and entire layers in a single step, the LVC concept enables rapid production of larger parts when compared to the effectively zero dimensional deposition of FDM.

A first-order analysis concluded that while maintaining an overall print resolution of 0.1 mm^2, the throughput of LVC is roughly $20\times$ greater than FDM when considering an available 1500 W power source and 100×100 mm build area. In cases where system power is limited, there is always a build volume for which FDM has a higher production rate than LVC, but for wattages above a reasonable threshold, the performance of LVC versus FDM continues to improve as the process is scaled to larger print areas.

Bench-level experiments proved the feasibility of the proposed process, and the next step is to implement LVC on a larger scale with closed loop temperature feedback. As a process where increasing the printed component footprint has minimal impact on production rate, LVC has the potential to open additive manufacturing to application areas, where thus far it has had only a minimal impact, and become an indispensible part of everyday life.

Acknowledgments

This work began as part of MIT 2.S998 Additive Manufacturing class.[14] The authors thank Professor A. John Hart and the course staff for their support. Professor Sanjay Sarma provided funding for the second-generation test setup.

Author Disclosure Statement

No competing financial interests exist.

References

1. Bellini A, Selcuk G, Bertoldi M. Liquefier dynamics in fused deposition. J Manuf Sci Eng 2004;126:237–246.
2. Kruth J-P, Leu MC, Nakagawa T. Progress in additive manufacturing and rapid prototyping. CIRP Ann Manuf Technol 1998;47:525–540.
3. Wachsmuth JP. Dissertation. Multiple independent extrusion heads for fused deposition modeling. Virginia Polytechnic Institute and State University 2008.
4. Brooks H, Rennie AEW, Abram TN, McGovern J, Caron F. Variable fused deposition modelling: Analysis of benefits, concept design and tool path generation. In: Proc. 5th International Conference on Advanced Research in Virtual and Rapid Prototyping, Leiria, Portugal: Taylor & Francis Group, 2011; pp. 511–517.
5. Keicher DM, Miller WD. U. S. Patent No. 6,268,584; 2001.
6. Horn TJ, Harrysson OLA. Overview of current additive manufacturing technologies and selected applications. Science Progress 2012;95:255–282.
7. HP. HP Multi Jet Fusion Technology. White paper. October 2014. Available from http://h41367.www4.hp.com/campaigns/ga/3dprinting/4AA5-5472ENW.pdf (accessed August 11, 2016).
8. Hansen CJ., *et al.* High-throughput printing via microvasculars multinozzle arrays. Adv Mater 2013;25:96–102.
9. Harper CA. Handbook of Plastics, Elastomers, and Composites, 2nd ed. New York: McGraw-Hill, 1996.
10. Freudenberger J, Göllner J, Heilmaier M, Mook G, Saage H, Srivastava V, *et al.* Materials science and engineering. In: Grote K-H, Antonsson EK, eds. Springer Handbook of Mechanical Engineering. Berlin, Heidelberg: Springer, 2009; pp. 208–212.
11. Fortes MA. Axisymmetric liquid bridges between parallel plates. J Colloid Interface Sci 1982;88:338–352.
12. Fortes MA. Deformation of solid surfaces due to capillary forces. J Colloid Interface Sci 1984;100:17–26.
13. Armillotta A. Assessment of surface quality on textured FDM prototypes. Rapid Prototyp J 2006;12:35–41.
14. Go J, Hart AJ. A framework for teaching the fundamentals of additive manufacturing and enabling rapid innovation. Addit Manuf 2016;10:76–87.

Address correspondence to:
Isaac M. Ehrenberg
Massachusetts Institute for Technology
77 Massachusetts Avenue
Room 35-205
Cambridge, MA 02139

E-mail: yitzi@mit.edu